Available online at www.sciencedirect.com

ScienceDirect

Journal of Taibah University for Science 11 (2017) 1245–1258

Journal of Taibah University for Science

www.elsevier.com/locate/jtusci

Full Length Article

Determination of optical parameters of zinc oxide nanofibre deposited by electrospinning technique

H.S. Bolarinwa [a,b,*], M.U. Onuu [b,c], A.Y. Fasasi [d], S.O. Alayande [d], L.O. Animasahun [a], I.O. Abdulsalami [e], O.G. Fadodun [d], I.A. Egunjobi [f]

[a] *Department of Physics, Electronics and Earth Sciences, Fountain University, Osogbo, Nigeria*
[b] *Department of Physics, University of Calabar, Calabar, Nigeria*
[c] *Department of Physics/Geology/Geophysics, Federal University Ndufu, Aliko, Ikwo, Nigeria*
[d] *Centre for Energy Research and Development, Obafemi Awolowo University, Nigeria*
[e] *Department of Chemical Sciences, Fountain University, Osogbo, Nigeria*
[f] *Department of Science Laboratory Technology, MAPOLY, Abeokuta, Nigeria*

Received 10 November 2016; received in revised form 2 January 2017; accepted 3 January 2017
Available online 16 January 2017

Abstract

Electrospun ZnO was deposited on a glass substrate from zinc acetate dihydrate ($Zn(CH_3COO)_2.2H_2O$) with polyvinyl acetate (PVAc) polymer dissolved in N, N, dimethyl formamide (DMF) and annealed in the presence of oxygen until organic molecules were decomposed. The resultant fibre was characterized using scanning electron microscope with energy dispersive spectrophotometry (SEMEDS), Fourier transform infrared (FTIR), and Rutherford backscattering spectroscopy (RBS). SEMEDS and FTIR exhibited a total decomposition of the organic precursor. The mean fibre width was found to be 260 nm, and fibre thickness was measured at 460 nm. XRD patterns indicate that ZnO was corundum with the hexagonal wurtzite structure. The crystallite size was determined by the Debye formula to be 54 nm. The optical analysis indicated that the percentage transmittance increased after calcination. The material band gap for this electrospun ZnO fibre was found to be 3.28 eV. The material optical parameters such as dispersion energy, average oscillator strength, and single oscillator strength were also calculated. The optical conductivity and dielectric plot demonstrated that the material conductivity and dielectric properties increase with increasing photon energy and increase sharply around the material energy bandgap. The Urbach tail analysis of the materials shows that they obey the Urbach rule. Therefore, the n-type electrospun ZnO fibre high refractive index is attributable to the presence of excess oxygen.

Keywords: Electrospinning; Calcined; Semiconductor; Nanofibre; Zinc Oxide

1. Introduction

Zinc oxide semiconductor materials have been widely used primarily due to low cost and outstanding chemical and physical properties [1]. ZnO is an n-type material having a wide band gap (3.21–3.42 eV) at room temperature. It is a group *II–VI* compound semiconductor having

* Corresponding author.
E-mail address: babdulhakeem@gmail.com (H.S. Bolarinwa).
Peer review under responsibility of Taibah University.

Production and hosting by Elsevier

http://dx.doi.org/10.1016/j.jtusci.2017.01.004

a stable wurtzite structure and large exciton bindng energy of 60 meV with lattice spacing $a = 0.325$ nm and $c = 0.521$ nm. It is a unique material that exhibits optical, semiconducting, pyroelectric and piezoelectric properties [2,3]. It has attracted serious research attention because of its applicability to wide applications such as light emitting diode [4,5], solar cells [6,7], chemical and gas sensors [8], ultraviolet (UV) light detector [9], stimulated emission with low loss and high gain [10], and transparent conducting oxide [11]. Due to these varied applications, several methods including thin films and polymeric approaches have been employed to deposit ZnO. Some of the thin film methods used include; chemical vapour deposition [12,13,14], chemical bath deposition [15], laser deposition [16,17], spray pyrolysis [18], magnetic sputtering [19], thermal oxidation [20], molecular beam epitaxy [21] and electrospraying [8]. ZnO fibre on the other hand has been synthesized using template [22] and electrospinning [23,24] methods.

The electrospinning method dates back to the work of Zeleny in 1914 and was previously termed "electrostatic spinning". This researcher found the technique to be useful for spinning polymer fibres having a small diameter [25]. This method, which uses the principle of electrostatics depends on electromotive force to form a fibre. This method has also been described as indispensable in the scientific and economic resurgence for developing nations [26]. Electrospinning has continued to gain serious research attention owing to its unique properties of the resultant nano/micro fibres (large surface area to volume ratio and cost effectiveness) [27,28]. ZnO nanofibres, including nanotube and nanorods [29] belong to the one-dimensional group of nanomaterials which are flexible in nature. ZnO nanofibres have demonstrated improved properties in photoconducting, semi-conducting and piezoelectric properties [30,31].

It has been reported that in modern day optoelectronics and optoelectronics design, a good knowledge of refractive index as a function of wavelength is important in predicting the photoelectric characteristics of a device [32]. Hence, an accurate knowledge of the optical and structural properties of electrospun ZnO fibres is important due to its very wide applicability in the analysis and design of optical and optoelectronics devices. Unfortunately, there are very large discrepancies in the optical properties of electrospun ZnO fibre reported from various studies. In view of this, reliable determination of the optical properties of the electrospun ZnO fibre is still paramount.

In this study, we synthesised ZnO nanofibres on glass substrate by electrospinning technique. The fibres have been characterized using X-ray diffraction analysis (XRD) for structural determination, scanning electron microscope (SEM-EDX) for morphology and composition. UV-Visible spectrophotometer and Fourier Transform Infrared Spectroscopy (FTIR) were also employed for determination of optical parameters as well as vibrational and stretching modes of the chemical bonds in the samples.

2. Materials and Methods

Poly(vinyl acetate) (PVAc) (Mw = 500,000 g by GPC), zinc acetate dihydrate ($Zn(CH_3COO)_2.2H_2O$) salt $\geq$ 99% assay from Sigma-Aldrich and anhydrous N-N-dimethylformamide $\geq$ 99.8% assay from Scharlau were used as precursor materials. 1 g of zinc acetate dihydrate salt with 1.6 g of polyvinyl acetate (PVAc) polymer were dissolved in 10 ml of anhydrous N, N, dimethyl formamide (DMF). The solution was stirred till it was homogenous. The glass substrate was precleaned using dilute hydrochloric (HCl) acid, ethanol and distilled water. The prepared solution was fed into the spinneret. The distance between the tip of the spinneret and the substrate was kept at 20 cm. 12 kV voltage was applied to the solution and the substrate attached to an aluminium foil was grounded. The solution was electrospun between 2 to 3 hours in order to have a thick fibre deposit. The deposited fibres on glass substrates were calcined at 700 °C in tubular furnace in the presence of oxygen. The as-spun and calcined fibre were later analysed for their chemical, structural, optical and electrical properties.

The scanning electron microscope TESCAN model equipped with Oxford instrument X-Max (EDS) was used to study the surface morphology and elemental composition of the electrospun and annealed fibres. Rutherford Backscattering analysis was carried out using the 1.7 MeV Ion Beam Accelerator at the Centre for Energy Research and Development, Obafemi Awolowo University, Ile-Ife, Nigeria to determine the elemental concentration and the thickness of the deposited fibres. The Fourier Transform Infrared (FTIR) was measured using a NICOLET S5 instrument from Thermo Scientific. The optical characterization was carried out using the Stellanet UV-visible Spectrophotometer model EP2000 (UV-VIS-NIR). ImageJ was used to determine the fibre diameter. The crystal structure and symmetry were analysed using Brucker D8 high resolution X-ray diffractometre (XRD).

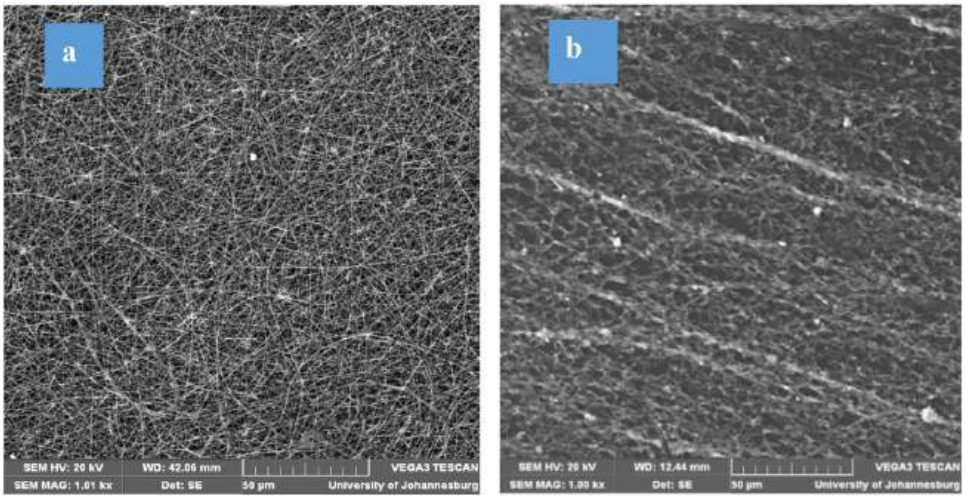

Fig. 1. The SEM images of the ZnO nanofibre (a) as-spun (b) calcined.

Table 1
Elemental composition of the calcine ZnO nanofibres determined by EDX.

Elements	Weight%	Atomic%	Compound	Formula
Si	44.65	32.58	95.51	SiO_2
Zn	3.60	1.13	4.49	ZnO
O	51.75	66.29		

Table 2
Concentration and thickness of the calcined ZnO from RBS after simulation.

Elements	Concentration	Bulk thickness (atm/cm^2)	Bulk thickness (nm)
Zn	0.136863	4.14E+17	460.215
O	0.863137		

3. Results and Discussion

3.1. Morphology

Fig. 1 shows the SEM image of the ZnO nanofibre. The average fibre diameter was found to decrease from 480 nm to 260 nm after calcination. The deposited nanofibres were non-woven in nature and are bead free. The difference in the measured mean fibre diameter observed in the as-spun and calcined material could be attributed to the removal of PVAc which served as a carrier for the metal oxide and other volatile inorganic constituents, such as acetate, during the calcination process.

3.2. Elemental and chemical analysis

The energy dispersive X-ray (EDX) analyses provide a way of analysing the chemical composition of materials. The EDX analysis of the calcined ZnO nanofibre is shown in Fig. 2 and Table 1. It is evident from the spectra that the fibres contained the desired elements. The presence of silicon in the calcined samples of Fig. 2 can be attributed to the glass substrate.

The RBS analysis gives the specific amount of each element present and most importantly the film's thickness that is necessary for optical data analysis. Previous findings have shown that the composition of a semiconductor plays an important role in its properties, hence the need to accurately determine and control the elemental make-up [33].

The result of the simulations of the RBS spectra using the SIMNRA software gave the amounts of specific elements and the thickness (in atoms/cm^2), which was then converted to nanometre. The RBS spectra for ZnO is shown in Fig. 3, and the analysis is presented in Table 2.

The distinct nature of the Zn peak from the spectra suggests that the electrospun nanofibre adheres firmly to the substrate. The RBS spectra suggests that decomposition of the starting precursor forms crystalline ZnO nanofibres. The spectra also show little or no trace of impurities from organic constituents, such as Carbon and Hydrogen or acetate.

The FTIR analysis of the studied ZnO electrospun nanofibres for the as-spun and calcined fibre is given in Fig. 4. The broad peak observed at 3513 cm^{-1} signifies the bonded O-H stretching frequencies of the alcohol for the as-spun nanofibre samples. These

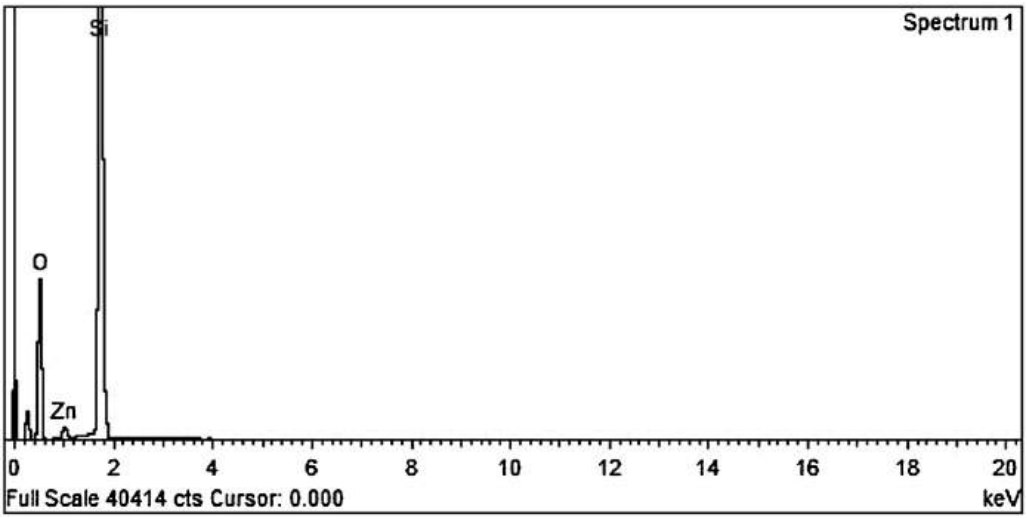

Fig. 2. Energy dispersive X-ray (EDX) for the calcined ZnO nanofibres.

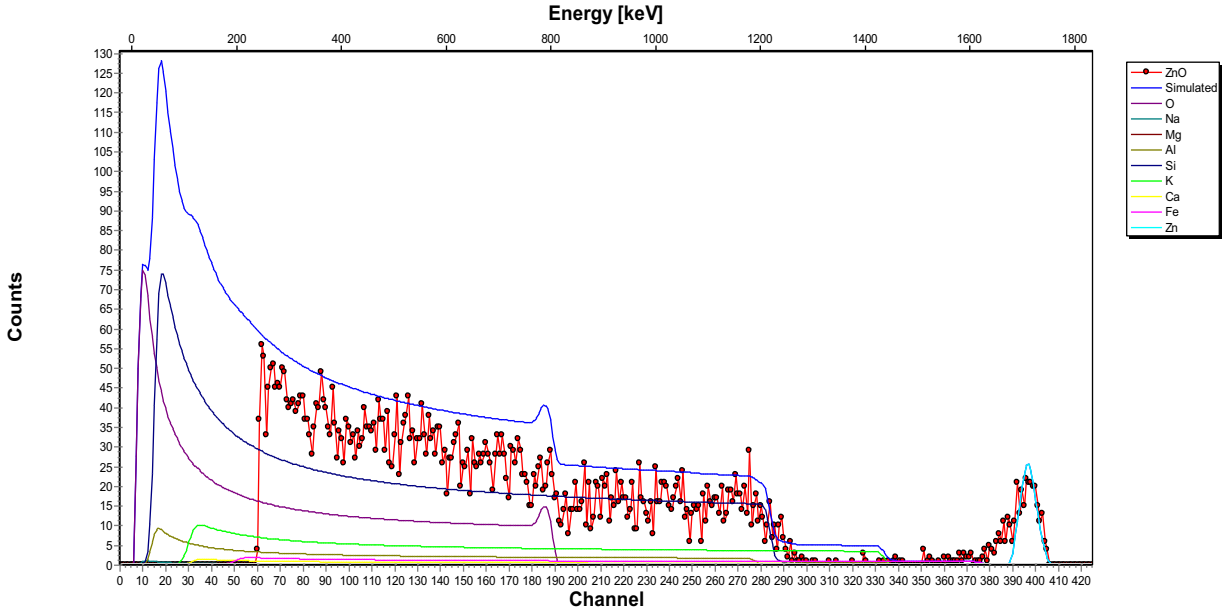

Fig. 3. Rutherford backscattering (RBS) spectrum of the calcined ZnO electrospun nanofibres.

O-H stretching could arise from the water molecule of the crystalline system of the $Zn(CH_3OO)_2.2H_2O$. The strong O-H stretching peaks observed for the calcine samples at 3686 cm^{-1} probably account for the non-bonded free O-H stretching frequencies in the calcine samples. The associated hypochromic shift (blueshift) observed for the calcine samples compared with the as-spun samples might be due to the effect of calcination on the sample. The double bond of CH, CH_2 or CH_3 observed at 2920 cm^{-1} in the as-spun fibres is attributed to the long chain of the PVAc polymer used. The absence of this bond in the calcined sample showed that the PVAc polymer had been removed from the sample as a result of the calcination. This further suggests a likely phase change from the amorphous to a crystalline phase.

3.3. Structural analysis

The X-ray diffraction patterns of the calcined sample was studied to confirm the crystallinity of the samples and to investigate its crystal structure. The ZnO spectra presented in Fig. 5 exhibit polycrystalline nature consisting of several diffraction peaks of hexagonal wurtzite structure with major diffraction peaks at [100],

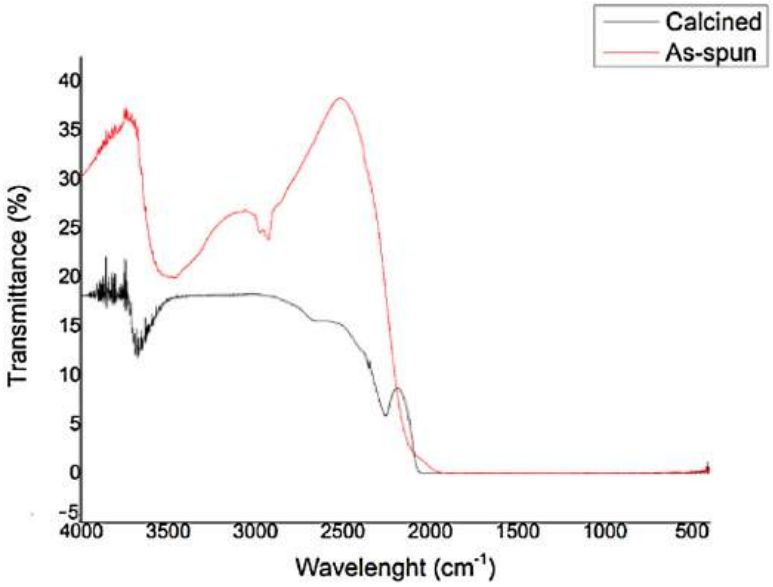

Fig. 4. FTIR spectra of ZnO nanofibres for as-spun and calcined sample.

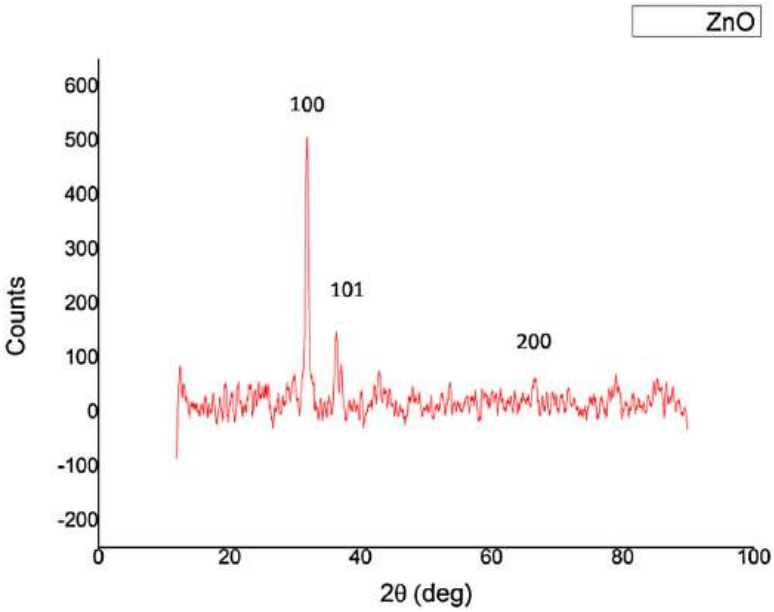

Fig. 5. XRD spectra of the calcined ZnO.

[101], and [200] corresponding to $2\theta = 32.58^{\circ}$, 36.98° and 67.20°, respectively, with the most pronounced peak indicating a preferred growth along the [100] direction. The observed peak matches the database of COD-Inorg REV140301 2015.07.06 corresponding to the entry 96-230-0451 [34]. The unit cell parameters of the ZnO as given by the reference database is $a = 3.2493$ Å $c = 5.2057$ Å and having a density of 5.677 g/cm^3 [35]. The matching phase and Rietveld refinement for the ZnO using the Match 3 software were performed, and the refinement showed that there is convergence with a reduced chi-square of 9.6 and weight average of 104.6. The average crystallite size of the fibre calculated using the Scherer formula given in equation 1 is 54 nm with lattice strain of 0.0024.

$$D = \frac{0.9\lambda}{B\cos\theta} \quad (1)$$

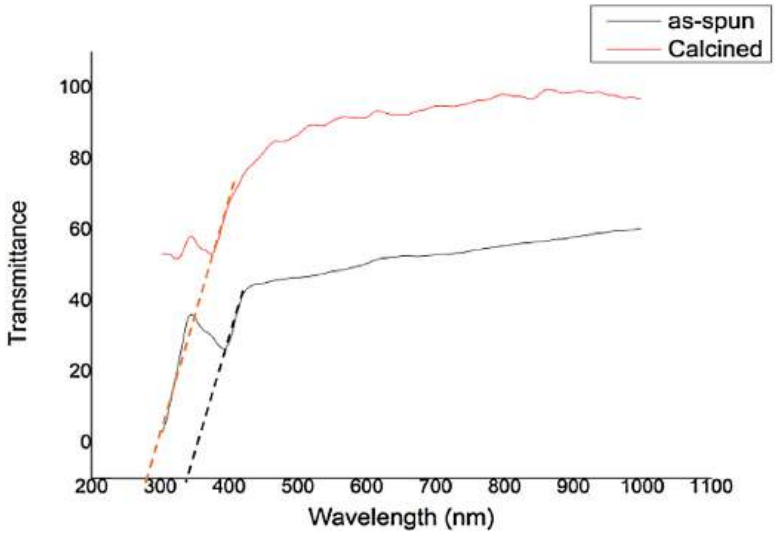

Fig. 6. Transmittance spectra of as-spun and calcine ZnO electrospun nanofibres.

3.4. Optical characterization

An increase in the percent transmittance was observed for the ZnO samples after calcination. This finding could be attributed to the decomposition of all the organic components presents in the as-spun fibres and the transformation from the amorphous state of the as-spun fibre to crystalline state as evidenced by the XRD results. Fig. 6 shows a cut off wavelength shift from 339 nm to 274 nm in the near UV region between the as-spun and calcined sample. The percent transmittance for ZnO increased from approximately 60% in the as-spun sample to approximately 98% in the calcine samples. As earlier stated; the decomposition of the organic polymer and the removal of the acetate from the $Zn(CH_3COO)_2.2H_2O$ to form crystalline ZnO provoked a reduction in the thickness which led to a rise in the transmittance [36,37]. The transmittance increased from the visible to the near-infrared region. A high transmittance value for zinc oxide was also reported previously, which implies that the ZnO deposited is very transparent as it allowed almost all the incident light to pass through it and absorbed very little as shown in Fig. 6.

The refractive index of semiconducting materials has been found to play an important role in their electrical and optical properties [38]. Material with a high refractive index have been known to trap incident rays [39].

The refractive index has been determined using equation 2 while the reflectance, as a function of wavelength, has been calculated from the transmittance data using equation 3. The variation in the refractive index as a function of the photon wavelength was obtained and plotted in Fig. 7.

$$n = \frac{1+\sqrt{R}}{1-\sqrt{R}} \quad (2)$$

$$R = 1 - (Texp(A))^2 \quad (3)$$

The refractive index was found to decrease gradually from shorter to longer wavelengths. This result is also supported by the findings previously reported [40]. The refractive index of the calcined zinc oxide was found to vary between 4.2 and 1.2 in the wavelength range of 300 nm to 1000 nm. This result lies within the ranges of 6.8 to 1.8 and 3.3 to 1.7 reported [41] for oxygen-deficient and nearly stoichiometric ZnO, respectively. However, in this study, oxygen was abundant due to the calcination process. Hence, the high refractive index of ZnO nanofibre may be attributed to excess oxygen.

The optical bandgap of materials is known as the minimum energy required by a semiconductor to excite a photon. The difference in the optical bandgap to the electrical bandgap lies majorly in the exciton binding energy. For material with very small exciton binding energy the optical bandgap and electrical bandgap are similar. To determine the optical bandgap of the materials deposited, we used the Tauc plot given in equation 4 and take n = 2, since ZnO exhibits direct bandgap [42,43].

$$\alpha = A\frac{(hv - E_g)^n}{hv} \quad (4)$$

A plot of $(\alpha hv)^n against\ hv$ gave the Tauc plot for the determination of the bandgap. The intersection of the linear fit with the hv axis at $(\alpha hv)^n = 0$ provided the optical band gap. The results from the Tauc plot are presented in Fig. 8. The obtained band gap for the ZnO was found

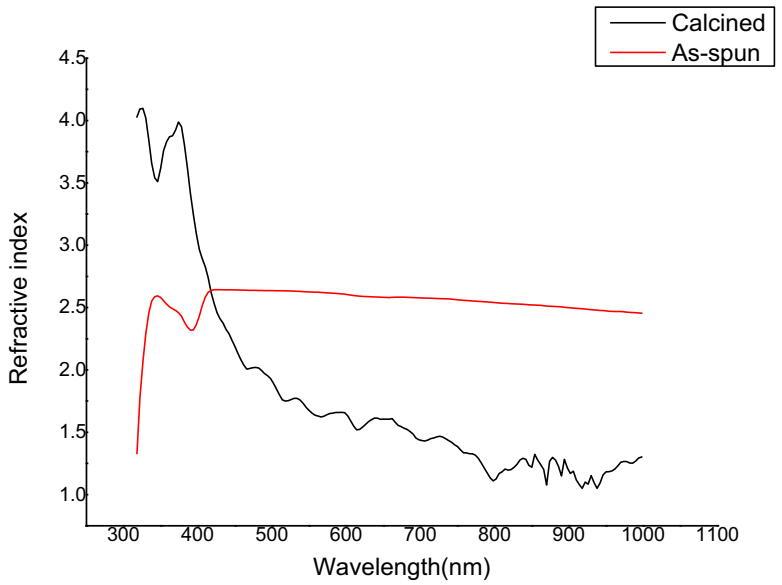

Fig. 7. Refractive index spectra for as-spun and calcined ZnO electrospun nanofibre.

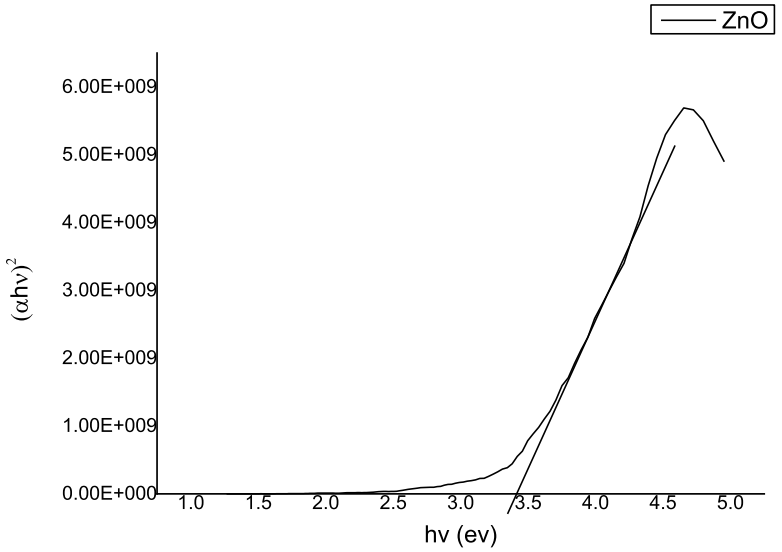

Fig. 8. Energy bandgap plot for the calcined ZnO nanofibre.

to be 3.28 eV, a value similar to that reported previously at 3.26 eV [42].

Oscillator's strength is one of the several parameters that are widely used in describing the atomic strength and optical molecular transition in materials [44]. Among the molecular and atomic parameters that are related to the optical strength are transition dipole moment [44]. The oscillator strength of a material is a dimensionless quantity which describes the probability of emission or absorption of electromagnetic radiation in the energy levels transitions of an atom or molecule [45] [46].

The spectroscopic data for the electrospun nanofibre were employed to derive their complex dielectric function. Dielectric imaginary and the real parts of the function ε" and ε', respectively, are related to the extinction coefficient "k"and refractive index "n" by equation 5 and 6, respectively,

$$\varepsilon' = n^2 - k^2 \quad (5)$$

$$\varepsilon'' = 2nk. \quad (6)$$

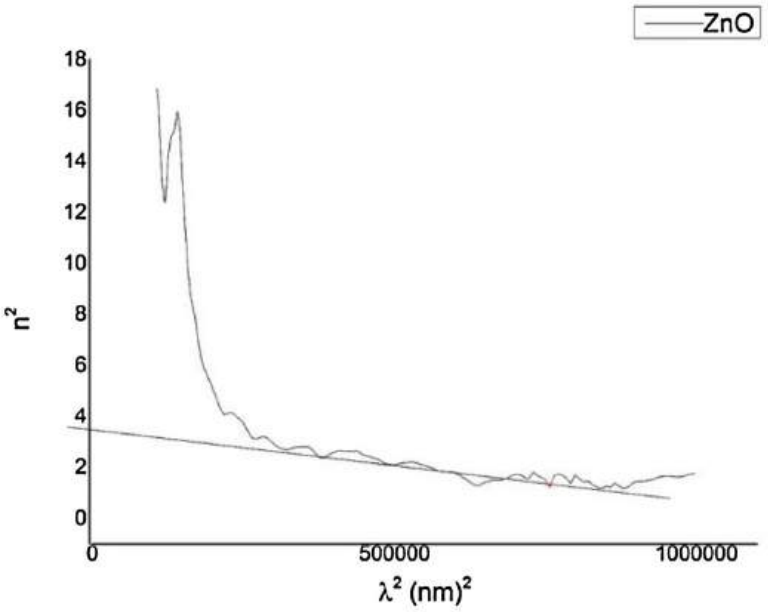

Fig. 9. Plot for determining the high frequency dielectric constant (ε_α) and density of state effective mass ratio $\left({}^{N_c}/_{m^*}\right)$ for the calcined ZnO nanofibre using equation 7..

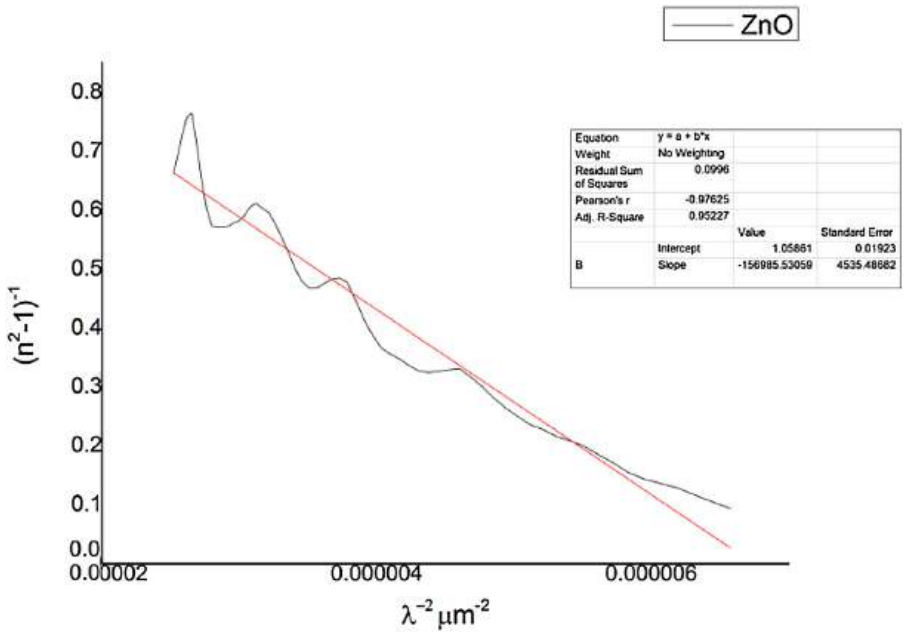

Fig. 10. Plot for determining the average oscillator parameters (λ_o) and average oscillator Strength (S_o), dispersion parameter ((E_o/S_o) for the calcined ZnO nanofibre using equation 8.

where $\varepsilon_{i,}$ $\varepsilon_{r,}$ k and n are the imaginary dielectric constant, real dielectric constant, extinction coefficient, and refractive index, respectively.

For the value of n far greater than k, ε' is approximately equal to n^2, the dependence of ε'' on λ can be examined using the relation [47] given by equation 7,

$$\varepsilon' = n^2 = \varepsilon_\infty - \left(\frac{e^2}{\pi c^2}\right)\left(\frac{N_c}{m^*}\right)\lambda^2 \qquad 7$$

where c is the speed of light, m^* is the effective mass of the carrier, N_c is the carrier density, e is the electronic charge, and ε_∞ is the high-frequency dielectric constant. To obtain the high frequency dielectric constantε_∞, a

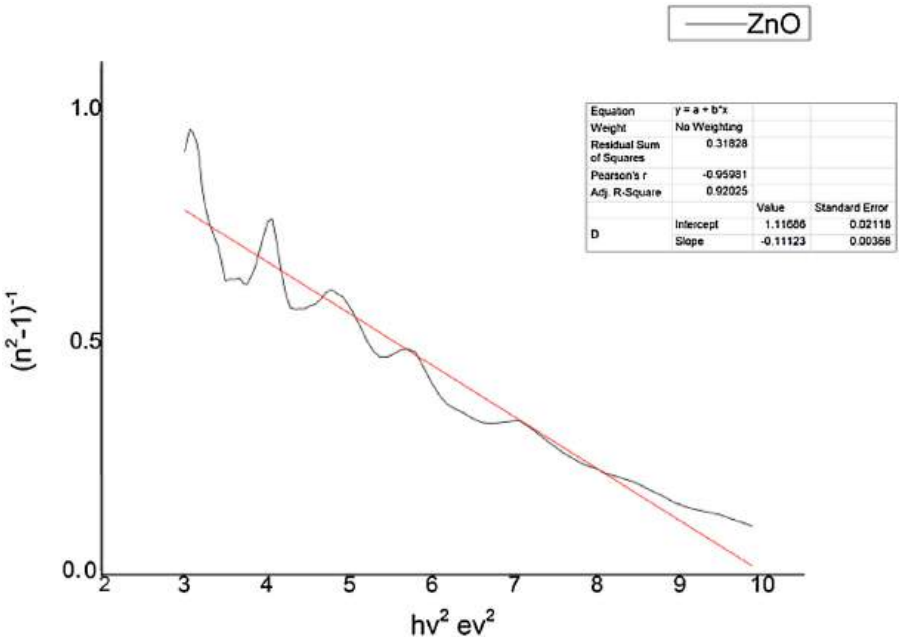

Fig. 11. Plot for determining the dispersion energy (E_d) dielectric constant (ε_o), single oscillator strength (E_{so}), and zero frequency refractive index (n_o) for the calcined ZnO nanofibre using equation 10..

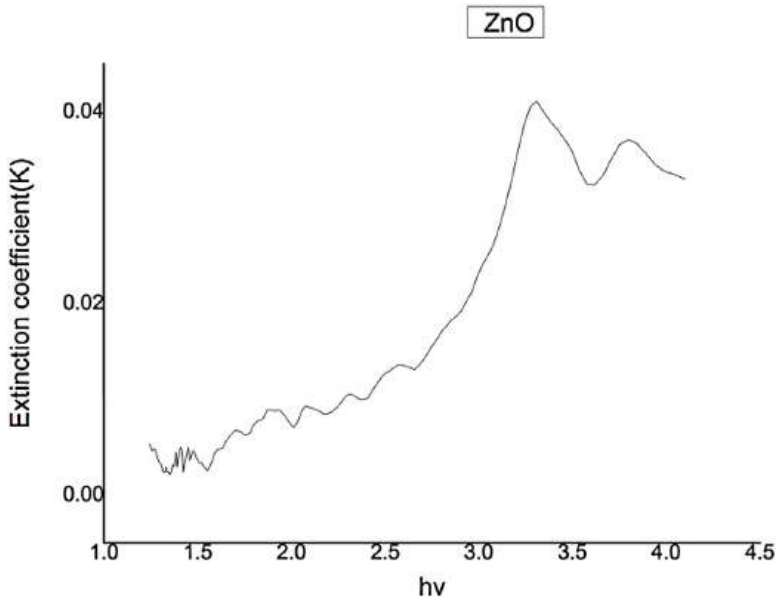

Fig. 12. Extinction coefficient Spectra for the calcined ZnO nanofibre.

graph of n^2 as a function of λ^2 was plotted, as shown in Fig. 9, and by extrapolating the linear part of the curve at higher wavelength to the n^2 axis at the intersection where $\lambda^2 = 0$, the value for the ε_∞ is obtained.

To evaluate various oscillator parameters, the long wavelength approximation of the single-term Sellmier relation [47]) is given:

$$n^2(\lambda) - 1 = \frac{S_o \lambda_o^2}{\left[1 - \left(\frac{\lambda_o}{\lambda}\right)^2\right]} \quad 8$$

λ_o is the average oscillator parameter *and* S_o is the average oscillator strength. Plotting of $(n^2(\lambda) - 1)^{-1}$ against

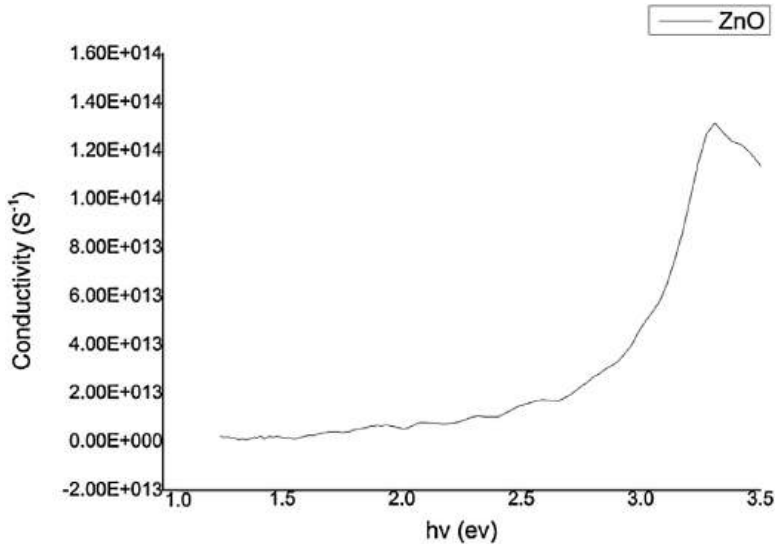

Fig. 13. Optical conductivity spectra for calcined ZnO nanofibre.

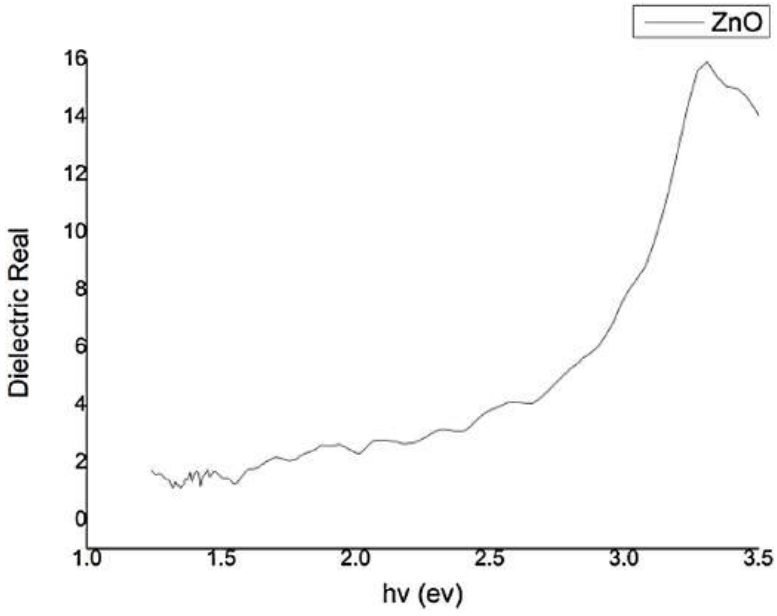

Fig. 14. Optical dielectric real part spectra for the calcined ZnO nanofibre.

λ^{-2} produces a straight line fit which gives the values of $1/S_o\lambda_o^2$ and $1/S_o$ from intercept and the slope, respectively. The dispersion parameter (E_o/S_o) for each sample is calculated using

$$E_o = \frac{\hbar c}{e\lambda_o} \quad 9$$

The plot is given in Fig. 10. The relationship between the refractive index and the photon energy is given by [47]

$$n^2(h\nu) - 1 = \frac{E_{so}E_d}{E_{so}^2 - (h\nu)^2} \quad 10$$

where E_{so} is the single oscillator strength and E_d is the dissipation energy. By linearizing the expression and plotting $(n^2\text{-}1)^{-1}$ against $(h\nu)^2$ and using the dielectric constant ε_o the zero-

$$\varepsilon_o = n_o^2 = 1 + {}^{E_d/E_{so}} \quad 11$$

frequency refractive index (n_o) was determined using the values of E_d and E_{so} determined from the slope (E_{so}/E_d)

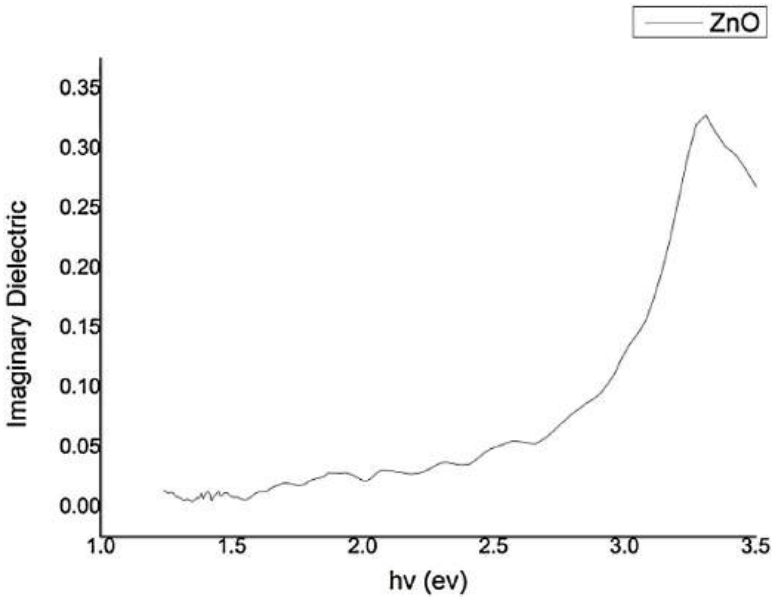

Fig. 15. Optical dielectric imaginary part spectra for the calcined ZnO nanofibre.

Table 3
Optical constants for the calcined ZnO electrospun nanofibre.

Optical parameters	Symbol	ZnO
Average oscillator strength	$\mathbf{S}_o$	6.37×10^{12} m^{-2}
Average oscillator parameter	$\boldsymbol{\lambda}_o$	0.37 (μm)
Dispersion parameter	$\mathbf{E}_o/\mathbf{S}_o$	1.23Ex 10^{-13} eVm^2
Single oscillator strength	$\mathbf{E}_{so}$	3.54 eV
Dispersion energy	$\mathbf{E}_d$	3.168 eV
High-frequency dielectric constant	$\boldsymbol{\varepsilon}_\infty$	3.29
Zero frequency dielectric constant	$\boldsymbol{\varepsilon}_o$	1.895367
Zero frequency refractive index	$\mathbf{n}_o$	1.38
Density of state effective mass ratio	$\mathbf{N}_c/\mathbf{m}^*$	1.1×10^{50} m/s^2 C^{-2}

and the intercept ($1/E_{so}E_d$). The plot is given in Fig. 11. The optical parameter constants obtained from the analysis are listed in Table 3.

Extinction coefficient k, given by equation 12 is a material parameter which defines how strongly it absorbs light at any given wavelength,

$$k = \frac{\alpha\lambda}{4\pi} \tag{12}$$

where k is the extinction coefficient, α = absorption coefficient and λ is the wavelength (Fig. 12).

The value of the extinction coefficient varies from 0.002 to 0.04 for the ZnO, as shown Fig. 14, which agrees with the result previously reported [43]. Knowing the value of the extinction coefficient and the refractive index of the material will allow the determination of the real and imaginary part of the dielectric constant of nanofibre materials. The relationship used is shown in equation 12. The optical conductivity of the material was estimated using equation 13. The relation between the conductivity and photon energy is given in Fig. 13 and that of the dielectric constant of photon energy in Fig. 14,

$$Conductivity = \frac{\alpha nc}{4\pi} \tag{13}$$

where α, n and c are absorption coefficient, refractive index and speed of light, respectively. The conductivity increases toward the high photon energy and increases sharply around the value of the bandgap energy. The graph of the dielectric shows the same trend as that of the conductivity. The sharp increase in the conductivity and dielectric constant around the bandgap can be attributed to the strong interaction between the photon and electron. It could also be seen that the dielectric characteristic for both the real and imaginary follow the same pattern with the value of real higher than that of the imaginary. The results obtained are similar to those previously reported [43], [48] for the dielectric property of ZnO (Fig. 15 and 16).

According to [49] "The exponential tail appears because disordered and amorphous materials produced localized states extended in the bandgap." The spectral dependence of the absorption edge in the low photon

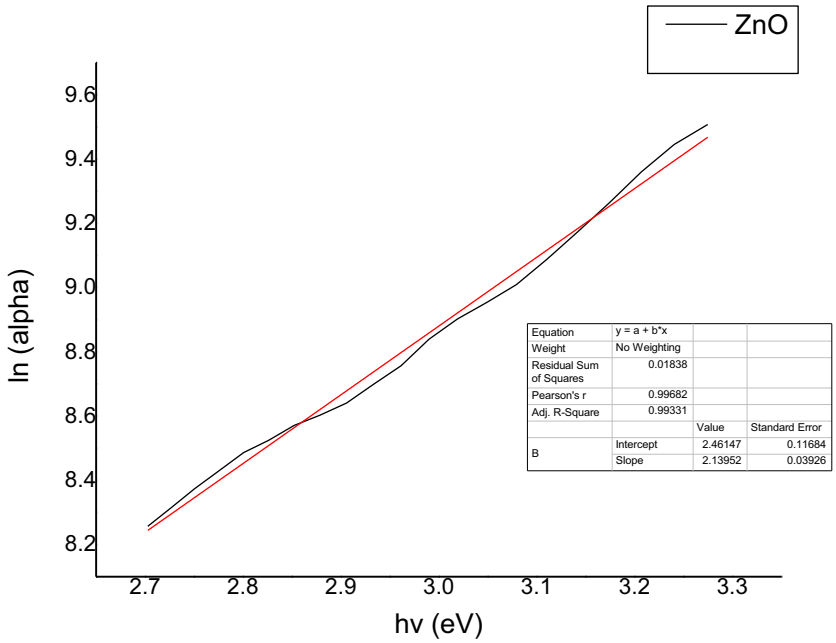

Fig. 16. Ubarch tail energy plot for the calcined ZnO nanofibre.

energy is assumed to obey the Ubarch rule given in equation 14

$$\propto (\nu) = \alpha_o exp\left(\frac{h\nu}{\Delta E}\right) \quad 14$$

where α_o is a constant, $h\nu$ is the photon energy and ΔE denotes "the width of the tail of localized states in the bandgap" (Urbach energy). By plotting ln(α) against $h\nu$, the inverse of the slope from the linear fit of the linear portions of the curves. Gives the Ubarch tail width energy of the localized state of the bandgap.

4. Conclusions

The electrospinning technique is a method of fibre deposition that has gained widespread acceptance owing to its unique properties, especially where a high specific large surface area to volume ratio exists. The deposited nanofibres of ZnO has gained widespread attention owing to its direct bandgap and high transmittance value. The ZnO nanofibre properties investigated include morphology, structure, chemical composition, refractive index, extinction coefficient, bandgap, transmittance, oscillators strengths and Urbach tail. The transmittance value of the ZnO nanofibre film between 56% and 99% in the visible region makes it a candidate for applications in the field of optoelectronics.

References

[1] Y.-Z. Gu, H.-L. Lu, Y. Geng, Z.-Y. Ye, Y. Zhang, Q.-Q. Sun, S.-J. Di, D.W. Zhang, Optical and microstructural properties of ZnO/TiO2 nanolaminates prepared by atomic layer deposition, Nanoscale Research Letters 8 (2013) 107.

[2] M. Anand, H.-S. Shim, Y.S. Kim, W.B. Kim, H.J. Kim, Structural and optical properties of Co- and Ti-ZnO composite nanofibre prepared by using an electrospinning method, Journal of the Korean Physical Society 53 (November (5)) (2008) 2423–2426.

[3] M. Taskin, J. Podder, Structural, optical and electrical properties of pure and co-doped ZnO nano fiber fhin films prepared by spray, Applied Science Reports 2 (3) (2014) 107–113.

[4] Y.Y. Liu, X.Y. Wang, Y. Cao, X.D. Chen, S.F. Xie, X.J. Zheng, H.D. Zeng, A flexible blue light-emitting diode based on ZnO nanowire/polyaniline heterojunctions, Journal of materials (2013).

[5] M.A. Abbasi, Z.H. Ibupoto, M. Hussain, O. Nur, M. Willander, The fabrication of white light-emitting diodes using the n-ZnO/NiO/P-GaN heterojunctions with enhanced luminescence, Nanoscale Research Letter 8 (320) (2013).

[6] Q. Zhang, C.S. Dandeneau, X. Zhou, G. Cao, ZnO naonostructure for dye-sentitized solar cells, Advanced Materials 21 (2009) 4087–4108.

[7] P. Tiwana, P. Docampo, M.B. Johnston, H.J. Snaith, L.M. Herz, electron mobility and injection dynamics in mesoporous ZnO, SnO2, and TiO2 films used in dye-sentitised solar cells, ACSNano 5 (6) (2011) 5158–5166.

[8] C.T. Pan, Y.C. Chen, C.C. Hsieh, C.H. Lin, C.Y. Su, C.K. Yen, Z.H. Liu, W.C. Wang, Ultrasonic sensing device with ZnO piezoelectric nanorods by selectivity electrospraying method, Sensors and Actuators A: Physical 216 (2014) 2318–2327.

[9] S.p. Ghosh, K.C. Das, N. Tripathy, G. Bose, D.H. kim, T.I. Lee, J.M. Myoung, J.P. Kar, Ultraviolet photodetection characteristics

of zinc oxide thin films and nanostructures, IOP Conf. Series: Matreial Science and Engineering (115) (2016).
[10] A.S. Gadallah, K. Nomenyo, C. Couteau, D.J. Rogers, G. Lerondel, Stimulated emission from ZNO thin film with high optical gain and low loss, Applied Physics Letter 102 (17) (2013).
[11] M.-C. Ju, S.-U. Park, J.-H. Koh, Comparative studies of Al-doped ZnO and Ga-doped ZnO transparent conducting oxide thin film, Nanoscale Research Letters 7 (639) (2012) 2–5.
[12] P.-C. Chang, Z. Fan, D. Wang, W.-Y. Tseng, W.-A. Chiou, J. Hong, J.G. Lu, ZnO nanowire synthesized by vapor Trapping CVD method, Chemical Mater,. vol. 16 (2004) 5133–5137.
[13] H. Liang, R.G. Gordon, Atmospheric pressure chemical vapor deposition of transparent conducting films of fluorine doped zinc oxide and their application to amorphous silicon solar cells, Journal of Material Science 42 (2007) 6388–6399.
[14] S. Kitova, I. Kalaglarski, S.R. Kazakov, Plasma enhanced chemical vapour deposition on thin ZnO layers on glass subtrate, Bulg. J. Phys. 40 (2013) 361–366.
[15] N.J. Blumenstein, C.G. Hofmiester, P. Lindemann, C. Haug, J. Baier, A. Leineweber, S. Walheim, C. Woll, T. Schimmel, J. Bill, Chemical bath deposition of textured and compact zinc oxide thin film on vinyl-terminated polystrene brushes, Beilstein Journal of Nanotechnology 7 (2015) 102–110.
[16] Y. He, J. Zhang, X. Yang, Q. Xu, C. Zhu, X. Hou, Study on pulsed laser ablation and deposition of ZnO thin films by L-MBE, Science in China Series E: Technological Sciences 50 (3) (2007) 290–301.
[17] S. Li, M. Chen, X. Liu, Zinc oxide porous nano-cages fabricated by laser ablation of Zn in ammonium hydroxide, Optics Express 22 (15) (2014) 18707–18714.
[18] E. Karber, T. Raadik, T. Dedova, J. Krustok, A. Mere, V. Mikli, M. Krunks, Photoluminescence of spray pyrolysis deposited ZnO nanorods, Nano Express 6 (359) (2011) 1–7.
[19] L.R. Damiani, R.D. Mansano, Zinc oxide thin films deposited by magnetron sputtering with various oxygen/argon concentration, Journal of Physics: Conference Series 370 (2012) 1–7.
[20] M.R. Khanlary, V. Vahedi, A. Reyhani, Synthesis and characterisation of ZnO nanowires by thermal oxidation of Zn thin films at various temperature, Molecules 17 (2012) 5021–5029.
[21] T. Makino, C.H. Chia, N.T. Taun, Y. Segawa, M. Kawasaki, A. Ohtomo, K. Tamura, H. Koinuma, Excition spectra of ZnO epitaxial layers on lattice-matched substrates grown with laser-molecular-beam epitaxy, Applied Physics Letter 76 (24) (2000) 3549–3551.
[22] B. Yu, F. Wang, W. Dong, J. Hou, P. Lu, J. Gong, Self-template synthesis of core-shell ZnO@ZIF-8 nanosheres and the photocatalysis under UV irradiation, Materials Letters 156 (2015) 50–53.
[23] A. Gupta, D.V. Nandanwar, S.R. Dhakate, Electrospun self assembled ZnO nanofibre structures for photocatalytic activity in natural solar radiations to degrade acid fuchsin dye, Advance Material letter 6 (8) (2015) 706–710.
[24] E.D. Adelowo, A.Y. Fasasi, M.O. Adeoye, S.O. Alayande, Structural and Optical Properties of Tin Doped Zinc Oxide Fibres Prepared By Electrospinning Technique, Chemistry and Materials Research (2013) 96–105.
[25] X. Zhang, M.R. Reagan, L.K. David, Electrospun Silk Biomaterial Scaffolds for Regenerative Medicine, Advanced Drug Delivery Review (2009) 988–1006.
[26] J. -h. He, Y. Liu, Electrospun Nanofibres and Their Applications, iSmither, Shrewsbury, 2008.
[27] W.E. Teo, S. Ramakrishna, A review on electrospinning design and nanofibre assemblies, Nanotecnology (2006) R89–R106.
[28] N. Bhardwaj, S.C. Kundu, Electrospinning: A fascinating fiber fabrication technique, Biotecnology Advances 28 (2010) 325–347.
[29] S. Ramakrishna, K. Fujihara, W.-E. Teo, T.-C. Lim, Z. Ma, An introduction to electrospinning and nanofibers, World Scientific Publishing Company Limited, Singapore, 2005.
[30] B.M. Sorayani, R. Bagherzadeh, M. Latifi, Fabrication of composite PVDF-ZnO nanofiber mats by electrospinning for energy scavenging application with enhanced efficiency, J Polym Res 22 (130) (2015).
[31] M. Imran, S. Haider, K. Ahmad, A. Mahmood, W.A. Al-masry, Fabrication and characterization of zinc oxide nanofibers for renewable energy applications, Arabian Journal of Chemistry (2013).
[32] O. Ostroverkhovaa, K.D. Singer, Space-charge dynamics in photorefractive polymers, Journal of Applied Physics 92 (4) (2002).
[33] A.E. Adeoye, E. Ajenifuja, B.A. Taleatu, Y.A. Fasasi, Rutherford backscattering spectometry analysis and structure properties of Znx Pb1-x S thin film deposited by chemical spray pyrolisis, Journal of Material (2015), p. 215210.
[34] S. Martin, G. Liangfeng, T. Satyanarayana, G. Feng, G. Marc, Simultaneous determination of several crystal structures from powder mixtures: the combination of powder X-ray diffraction, band-target entropy minimization and Rietveld methods, Journal of Applied Crystallography 47 (2) (2014) 659–667.
[35] S. Martin, G. Liangfeng, T. Satyan, T. Satyanarayana, G. Feng, G. Marc, Simultaneous determination of several crystal structures from powder mixtures: the combination of powder X-ray diffraction, band-target entropy minimization and Rietveld methods, Journal of Applied Crystallography 47 (2) (2014) 659–667.
[36] Y.-Y. Cho, C. Kuo, Optical and electrical characterization of electrospun Al-doped zinc oxide nanofibers as transparent electrodes, J. Mater. Chem. C 4 (2016) 7649–7657.
[37] Y. Liao, T. Fukuda, S. Wang, Electrospun metal oxide nanofibers and their energy application, in: M.M. Rahman, M. Abdullah (Eds.), Nanofiber research – Reaching new heights, InTech Open, 2016, pp. 169–190.
[38] N. Baydogan, T. Ozdurmusoglu, H. Cimenoglu, A.B. Tugrul, Refractive index and extinction coefficient of ZnO:Al thin films derived by sol-gel dip coating technique, Defect and Diffusion Forums (2013) 290–293.
[39] M. Ma, F.W. Mont, X. Yan, J. Cho, F. Schubert, G.B. Kim, C. Sone, Effects of the refractive index of the encapsulant on the light-extraction efficiency of light-emitting diodes, OPTICS EXPRESS 19 (September (S5)) (2011) A1135–A1140.
[40] I.A. Ezenwa, Synthesis and optical characterization of zinc oxide thin film, Research Journal of Chemical Sciences (2012) 26–30.
[41] S.H. Mohamed, Synthesis, structural and elliposmetric evaluation of oxygen-deficient and nearly stiochiometric zinc oxide and indium oxide nanowire/nanoparticles, Philosophical Magazine (2011) 3598–3612.
[42] H. Afifi, M. Abdel-Naby, S. El-Hefnawie, A. Eliewa, N. Ahmad, Optical and Electrical Properties of Zinc Oxide thin film prepared by spray pyrolysis, Iraqi Journal of Applied Physics (2010) 23–28.
[43] F. Yakuphanoglus, S. Ilican, M. Caglarb, Y. Cagla, The determination of the optical band and optical constants of non-crystalline and crystalline ZnO thin films deposited by spray pyrolysis, Journal of Optoelectronics and Advanced Materials 9 (July (7)) (2007) 2180–2185.

[44] R.C. Hilborn, Einstein coefficients, cross sections, f values, dipole moments, and all that, Am. J. Phys. 50 (1982) 982–986.
[45] J.W. Robinson, Atomic Spectroscopy, second ed., MARCEL DEKKER, Incorporated, New York, 1996.
[46] W. Demtröder, Laser Spectroscopy: Basic Concepts and Instrumentation, Springer, Berlin, 2003, p. 31.
[47] A.Y. Fasasi, B.D. Ngom, J.B. Kana-Kana, R. Bucher, M. Maaza, C. Theron, U. Buttner, Synthesis and characterisation of Gd-doped BaTiO3 thin films prepared by laser ablation for optoelectronic applications, Journal of Physics and Chemistry of Solids 70 (10) (2009) 1322–1329.
[48] A.-S. Gadallah, M.M. El-Nahass, Structural, optical constants and photoluminescence of ZnO thin films grown by sol-Gel spin coating, Advances in Condensed Matter Physics (2013) 1–11.
[49] S.J. Ikhmayies, R.N. Ahmad-Bitar, A study of the optical bandgap energy and Urbach tail of spray-deposited CdS:In thin films, Journal of Material Research and Technology (2013) 221–227.